THE JOURNAL OF PHYSICAL CHEMISTRY B

ARTICLE

pubs.acs.org/JPCB

# High-Accuracy Vapor Pressure Data of the Extended $[C_nC_1im][Ntf_2]$ Ionic Liquid Series: Trend Changes and Structural Shifts

Marisa A. A. Rocha,[†] Carlos F. R. A. C. Lima,[†] Lígia R. Gomes,[§] Bernd Schröder,[‡] João A. P. Coutinho,[‡] Isabel M. Marrucho,[‡,∥] José M. S. S. Esperança,[∥] Luís P. N. Rebelo,[∥] Karina Shimizu,[#] José N. Canongia Lopes,[∥,#] and Luís M. N. B. F. Santos*[,†]

[†]Centro de Investigação em Química, Departamento de Química e Bioquímica, Faculdade de Ciências da Universidade do Porto, R. Campo Alegre 687, P-4169-007 Porto, Portugal

[‡]CICECO, Departamento de Química, Universidade de Aveiro, P-3810-193 Aveiro, Portugal

[§]CIAGEB, Faculdade de Ciências da Saúde da UFP, Universidade Fernando Pessoa, R. Carlos da Maia 296, P-4200-150 Porto, Portugal

[∥]Instituto de Tecnologia Química e Biológica, ITQB2, Universidade Nova de Lisboa, Av. República, Apartado 127, P-2780-901 Oeiras, Portugal

[#]Centro de Química Estrutural/IST, Av. Rovisco Pais, P-1049-001 Lisboa, Portugal

Supporting Information

**ABSTRACT:** For the first time, two distinct trends are clearly evidenced for the enthalpies and entropies of vaporization along the $[C_nmim][Ntf_2]$ ILs series. The trend shifts observed for $\Delta_l^g H_m^o$ and $\Delta_l^g S_m^o$, which occur at $[C_6mim][Ntf_2]$, are related to structural modifications. The thermodynamic results reported in the present article constitute the first quantitative experimental evidence of the structural percolation phenomenon and make a significant contribution to better understanding of the relationship among cohesive energies, volatilities, and liquid structures of ionic liquids. A new Knudsen effusion apparatus, combined with a quartz crystal microbalance, was used for the high-accuracy volatility study of the 1-alkyl-3-methylimidazolium bis(trifluoromethylsulfonyl)imide series ($[C_nmim][Ntf_2]$, where $n$ = 2, 3, 4, 5, 6, 7, 8, 10, 12). Vapor pressures in the (450−500) K temperature range were measured, and the molar standard enthalpies, entropies, and Gibbs energies of vaporization were derived. The thermodynamic parameters of vaporization were reported, along with molecular dynamic simulations of the liquid phase structure, allowing the establishment of a link between the thermodynamic properties and the percolation phenomenon in ILs.

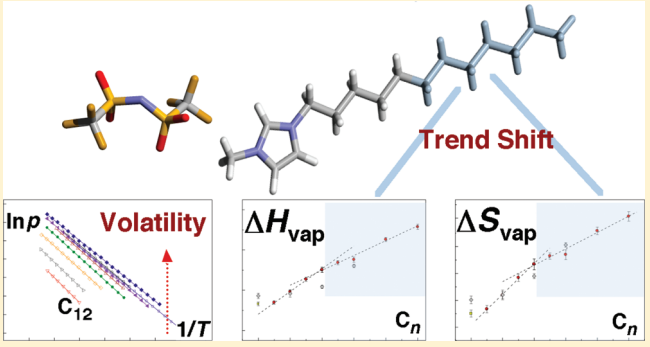


## 1. INTRODUCTION

Many properties of ionic liquids, for example, melting temperature, acidity and basicity, surface tension, or solubility in water and organic solvents can be adjusted by modifying the cations, anions, or both. Many authors have claimed that ionic liquids share common characteristics such as moderate-to-low electrical conductivity, moderate-to-high viscosity, good thermal stability, and extremely low vapor pressure at room temperature. However, extensive studies on the properties of ILs in the past decade[1] have shown that almost none of these properties are shared across the IL range; therefore, none of them can be considered in and of themselves as a defining characteristic of an ionic liquid.

Over recent years, a growing number of applications for these fluids have been developed. Nowadays, they can be used in multiple industrial processes,[2] including, cellulose processing,[3,4] gas handling, solar energy conversion,[5] and waste recycling. Besides their advantages for specific applications (catalytic activity, solvent effects, separation phenomena), ionic liquids have been designated as "green solvents" because of their low volatility, which prevents their spread into the atmosphere. Nonetheless, it has been also found that they are not free of toxicity, with aquatic toxicities at the same level of some organic solvents,[6] causing some controversy concerning the application of the "green solvent" label.[7] In fact, their extremely low volatilities limit the range of techniques available for their separation and purification, reducing the options for multiple recycling cycles during or after the manufacturing process as well as their recovery, storage, and so on.

It has been discovered that, at moderate temperatures, some ionic liquids may present a range of non-negligible vapor

**Received:** May 26, 2011
**Revised:** July 31, 2011
**Published:** August 04, 2011

pressures.[8] Earle et al.[8] have also shown that by fine-tuning the thermal stability of those ionic liquids it was possible to achieve their distillation.[9] Hence, during the past decade, the volatility of ionic liquids has been the subject of several studies to determine their vapor pressure and vaporization enthalpy with accuracy.[10] Additional information regarding these properties should shed light on the structural arrangement of the ions in the liquid phase, their cohesive energy, as well as the nature of the corresponding vapor phase. Moreover, accurate thermodynamic parameters of vaporization equilibrium are required to validate the models (force fields) used to describe ionic liquids in different simulation techniques (quantum and molecular mechanics, molecular dynamics (MD), Monte Carlo) and to anchor the parameters used in $P-V-T$ equations of state and other semiempirical prediction methods.

Previous works in this field focused on indirect determinations of vapor pressure at moderate temperatures (generally >400 K). Several approaches to measuring and predicting this quantity have been proposed, including MD simulations.[11] Direct experimental determinations have been carried out by the integral Knudsen effusion method,[12] transpiration method,[13] mass spectrometry,[14,15] high-precision vacuum vaporization drop microcalorimetry,[16] and thermogravimetry.[17] Despite all of these efforts, most of them centered on the determination of the vapor pressure and enthalpy of vaporization of ionic liquids of the 1-alkyl-3-methylimidazolium bis(trifluoromethylsulfonyl)imide family, $[C_nC_1im][Ntf_2]$, discrepancies still remain within the state-of-the-art data. Because the majority of the experiments have to be performed at moderate-to-high temperatures (>400 K and below the decomposition temperatures of the ionic liquids) and under very low pressure conditions, most of the expected systematic errors are related to the purity and thermal stability of the ionic liquid during the measurement.

In this work, we present for the first time a high-accuracy study of the volatility of 1-alkyl-3-methylimidazolium bis(trifluoromethylsulfonyl)imide ionic liquids ($[C_nC_1im][Ntf_2]$ with $n$ = 2, 3, 4, 5, 6, 7, 8, 10, 12). The vapor pressure of each pure ionic liquid has been determined as a function of temperature in the [440−495] K range using a new quartz microbalance Knudsen effusion apparatus[18] and applying a methodology developed for this purpose. On the basis of the experimental results, the standard molar enthalpy, entropy, and Gibbs energy of vaporization have been derived. These properties were used to evaluate and rationalize the relationship among cohesive energy, volatility, and structural organization in the liquid phase of this homologous series of ionic liquids.

## 2. EXPERIMENTAL SECTION

**2.1. Synthesis, Purification, and Characterization of Compounds.** The ionic liquids used in this work, the 1-alkyl-3-methylimidazolium bis(trifluoromethylsulfonyl)imide series, $[C_nC_1im][Ntf_2]$ ($n$ = 2, 3, 4, 5, 6, 8, 10, 12), were synthesized and purified at QUILL (The Queen's University Ionic Liquid Laboratories, Belfast) following reported procedures.[19] The sample 1-heptyl-3-methylimidazolium bis(trifluoromethylsulfonyl)imide, $[C_7C_1im][Ntf_2]$ was purchased from IOLITEC with a stated purity of better than 99%.$^1$H NMR analysis showed no major impurities except for the presence of water. Chloride analysis using a chloride electrode and the standard addition method indicated chloride contents smaller than 150 ppm.

Before each effusion experiment, the ionic liquids were dried under reduced pressure (<10 Pa) and stirred constantly for a minimum of 48 h at 373 K to reduce the presence of water or other volatile contents. The purity of the samples was verified by $^1$H and $^{19}$F NMR spectroscopy. Karl Fischer titration of the degassed samples revealed <100 ppm of water before the sample was inserted in the vacuum chamber. Inside the vacuum chamber, an additional cleaning experiment was performed at high temperature that reduces the water level in the sample inside the Knudsen cell. It was found that the differences in the derived vapor pressure (in different sets of data with the same IL obtained in independent experiments) do not correlate with the initial water content. The hypothetical effect of the water mass loss in the gravimetric weighing is considered to be negligible.

**2.2. Quartz Crystal Microbalance Knudsen Effusion Apparatus.** The vapor pressure of each ionic liquid was measured as a function of temperature using a new Knudsen effusion apparatus combined with a quartz crystal microbalance, KEQCM, recently described by Santos et al.[18] This simultaneous gravimetric and quartz crystal microbalance mass loss detection technique enables us to decrease both sample size and effusion times while achieving temperatures of up to 650 K. The combination of two mass loss determination techniques permits the instrument to measure vapor pressures from 0.005 to 1 Pa. The temperature step effusion procedure allows for vapor pressure measurements at different temperatures in one single experiment. The apparatus is essentially a closed system under high vacuum, comprising a quartz crystal positioned above the effusion cell; it is placed in an oven at controlled temperature. Like a typical Knudsen effusion experiment, the system is kept at high vacuum, allowing free effusion of the vapor from the cell, and at a fixed temperature, $T$. The temperature is controlled within a temperature fluctuation of $\pm(1 \times 10^{-2})$ K, measured with a resolution better than $1 \times 10^{-3}$ K and with an overall uncertainty better than $\pm(2 \times 10^{-2})$ K along the entire working temperature range. At the working temperature, the quartz crystal microbalance is not sensitive to the water. The vapor pressure data obtained with this apparatus presents a maximum deviation of 1%.

At the temperature $T$, the mass $m$ of the sample vaporized from the effusion cell, during the time period $t$, is related to the equilibrium vapor pressure of the liquid compound by the Knudsen equation

$$p(T) = (\Delta m/\Delta t)_T \cdot (1/A_o \cdot w_o) \cdot (2\pi RT/M)^{1/2} \quad (1)$$

where $M$ is the molar mass of the sample, $R$ is the gas constant ($R$ = 8.314472 J·K$^{-1}$·mol$^{-1}$), $A_o$ is the area of the orifice, and $w_o$ is the transmission probability factor ($w_o = \{1 + (l/2r)\}^{-1}$). The relative atomic masses used were those recommended by the IUPAC Commission in 2007.[20]

## 3. RESULTS AND DISCUSSION

The detailed experimental results for vapor pressure, $p$, obtained in the KEQCM for the nine $[C_nC_1im][Ntf_2]$ ionic liquids as a function of temperature, are given in Table S1 of the Supporting Information. Figure 1 represents $\ln(p/Pa)$ as a function of $\{(1/T)/K^{-1}\}$. The higher working temperature was limited by the thermal stability of the ILs, and the lower temperature was limited by the mass loss detection limited. The vapor pressure experimental results were fitted to the Clarke and

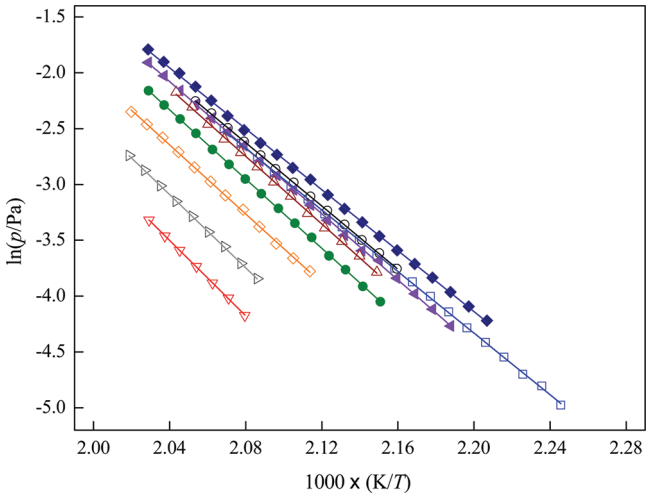


**Figure 1.** Plot of $\ln(p/\mathrm{Pa}) = f[(1/T)/\mathrm{K}^{-1}]$ for each studied ionic liquid: □, (blue), $[C_2C_1im][Ntf_2]$; ◆ (blue),$[C_3C_1im][Ntf_2]$; ○ (black), $[C_4C_1im][Ntf_2]$; ◀ (pink), $[C_5C_1im][Ntf_2]$; △ (brown), $[C_6C_1im]$-$[Ntf_2]$; ● (green), $[C_7C_1im][Ntf_2]$; ◇ (orange), $[C_8C_1im][Ntf_2]$; ▷ (gray), $[C_{10}C_1im][NTf_2]$; ▽ (red), $[C_{12}C_1im][Ntf_2]$.

Glew eq 2[21]

$$R\ln\left[\frac{p(T)}{p^{o}}\right] = -\frac{\Delta_l^g G_m^o(\theta)}{\theta} + \Delta_l^g H_m^o(\theta)\cdot\left(\frac{1}{\theta}-\frac{1}{T}\right) + \Delta_l^g C_{p,m}^o\cdot\left[\frac{\theta}{T}-1+\ln\left(\frac{T}{\theta}\right)\right] \quad (2)$$

where $p$ is the vapor pressure, $p^o$ is the standard pressure ($p^o = 10^5$ Pa), $\theta$ is a selected reference temperature, $R$ is the molar gas constant ($R = 8.314472\ \mathrm{J\cdot K^{-1}\cdot mol^{-1}}$), $\Delta_l^g G_m^o$ is the standard molar Gibbs energy of vaporization at the selected reference pressure, $\Delta_l^g H_m^o$ is the standard molar enthalpy of vaporization, and $\Delta_l^g C_{p,m}^o$ is the difference between the heat capacities of the gaseous and of the liquid phases $[\Delta_l^g C_{p,m}^o = C_{p,m}^o(g) - C_{p,m}^o(l)]$. The values of $\Delta_l^g C_{p,m}^o$ were estimated considering the same temperature for all ILs, $T = 388$ K, and the available literature values for $C_{p,m}^o(l)$ and $C_{p,m}^o(g)$.[22−25] Hence, the values of $\Delta_l^g C_{p,m}{}^o$ ($T = 388$ K) were estimated using the linear fitted function ($\Delta_l^g C_{p,m}^o = -5.40\cdot n(\mathrm{C}) - 100.47$) derived from fitting the literature data of $\Delta_l^g C_{p,m}^o(T = 388\ \mathrm{K})$ as a function of the cationic alkyl chain length. (See Figure S1 of the Supporting Information.) A more detailed explanation of the $\Delta_l^g C_{p,m}^o$ ($T = 388$ K) estimate for the nine studied ionic liquids is presented as Supporting Information. Taking the values of $\Delta_l^g C_{p,}^o$m (Table 1) into account, the standard molar enthalpies, entropies, and Gibbs energies of vaporization at reference temperature, $T = 298.15$ K, were derived. Table 1 lists the derived standard ($p^o = 10^5$ Pa) molar enthalpies, entropies, and Gibbs energies of vaporization at the mean temperature, <$T$>, and at reference temperature, $T = 298.15$ K, as derived from the fitting of eq 2 and related to each other by the following eq 3

$$\Delta_l^g G_m^o(T) = -RT\ln\left[\frac{p(T)}{p^o}\right] = \Delta_l^g H_m^o(T) - T\cdot\Delta_l^g S_m^o(T) \quad (3)$$

The plots of $\ln(p/\mathrm{Pa})$ as a function of $\{(1/T)/\mathrm{K}^{-1}\}$ presented in Figure 1 show that the volatility of the $[C_nC_1im][Ntf_2]$ ionic liquids decreases along the homologous series, from $[C_3C_1im][Ntf_2]$ to $[C_{12}C_1im][Ntf_2]$. $[C_2C_1im][Ntf_2]$ is an exception to this trend, with lower volatilities than $[C_3C_1im][Ntf_2]$ in the measured temperature range.

Zaitsau et al.[12] also measured the vapor pressure of $[C_2C_1im][Ntf_2]$, $[C_4C_1im][Ntf_2]$, $[C_6C_1im][Ntf_2]$ and $[C_8C_1im][Ntf_2]$ by the effusion Knudsen method. Figure S2, presented as Supporting Information, compares their data with the present results. A reasonable agreement between the two data sets is observed. Nevertheless, small, systematic deviations between the data will affect the derived thermodynamic properties of vaporization, as discussed below.

The thermodynamic properties of vaporization, at $T = 298.15$ K, as derived from the data presented by Zaitsau et al.[12] were recalculated in this work using the same $\Delta_l^g C_{p,m}^o$. The graphic representation of the standard molar Gibbs energies of vaporization, $\Delta_l^g G_m^o(298.15\ \mathrm{K})$, as a function of the alkyl side chain length of the cation, $n(\mathrm{C})$, is presented in Figure 2. The Figure shows that the thermodynamic parameters of vaporization for $[C_2C_1im][Ntf_2]$ and $[C_4C_1im][Ntf_2]$ are in reasonable agreement, whereas those for $[C_6C_1im][Ntf_2]$ and $[C_8C_1im][Ntf_2]$ show differences of around $-5\ \mathrm{kJ\cdot mol^{-1}}$.

The volatility is directly related to the $\Delta_l^g G_m^o(298.15\ \mathrm{K})$: as this quantity rises, with increasing $n(\mathrm{C})$, the volatility along the ionic liquid homologous series falls. Figure 2 depicts an ill-defined trend in the literature data[12] in contrast with the steady increase in $(1.9 \pm 0.1)\ \mathrm{kJ\cdot mol^{-1}}$ per each methylene group $(-CH_2-)$ from $[C_3C_1im][Ntf_2]$ to $[C_{12}C_1im][Ntf_2]$ obtained in the present work. At the reference temperature, $[C_2C_1im][Ntf_2]$ and $[C_3C_1im][Ntf_2]$ exhibit the highest volatilities in the series.

The standard molar enthalpies of vaporization, $\Delta_l^g H_m^o(298.15\ \mathrm{K})$, as a function of the alkyl side chain length of the cation, $n(\mathrm{C})$, are represented in Figure 3.

The previous literature data of $\Delta_l^g H_m^o(298.15\ \mathrm{K})$ are in reasonably good agreement with the present results, with the exception of the value for $[C_6C_1im][Ntf_2]$, which is clearly lower. Santos et al.[16] performed direct measurements of the enthalpies of vaporization by Calvet microcalorimetry. Figure S3 (Supporting Information) presents a detailed comparison of those data with the current ones. Considering the associated uncertainty, only the $\Delta_l^g H_m^o(298.15\ \mathrm{K})$ results for $[C_2C_1im][Ntf_2]$ and $[C_4C_1im][Ntf_2]$ from Santos et al.[16] are in reasonable agreement with the present set of results or most of the results found in the literature.[12,16] The systematically higher results measured by Calvet microcalorimetry[16] may be attributable to a systematic error arising from the high experimental temperatures of the calorimetric measurements, some sample decomposition in the vaporization experiments, or both.

The current results show, for the first time, two distinct trends for the enthalpy of vaporization along the series. In the $[C_3C_1im][Ntf_2]$ to $[C_6C_1im][Ntf_2]$ range, $\Delta_l^g H_m^o(298.15\ \mathrm{K})$ increases $(5.5 \pm 0.2)\ \mathrm{kJ\cdot mol^{-1}}$ per $-CH_2-$ group added to the alkyl side chain of the cation. Between $[C_6C_1im][Ntf_2]$ and $[C_{12}C_1im][Ntf_2]$, the corresponding growth accounts only for $(3.7 \pm 0.2)\ \mathrm{kJ\cdot mol^{-1}}$. The decrease in the$\Delta_l^g H_m^o$ along the series (from 5.5 to 3.7 $\mathrm{kJ\cdot mol^{-1}}$·per $-CH_2-$ group), indicates a falling the contribution per methylene group to the cohesive energies from $[C_6C_1im][Ntf_2]$ to $[C_{12}C_1im][Ntf_2]$. It is interesting to observe that the enthalpies of vaporization, $\Delta_l^g H_m^o$, obtained for $[C_2C_1im][Ntf_2]$ and $[C_3C_1im][Ntf_2]$ are similar, which points out a balance between the decrease in electrostatic interaction and the increase in the intermolecular

**Table 1. Parameters of Clarke and Glew Equation Fitted from the Vapor Pressure Results and the Derived Standard Molar Entropy of Vaporization for Each Studied IL at the Reference Temperature, $\theta$, and at the Standard Pressure, $p^o = 10^5$ Pa**

| $T$ interval/K | $\theta$/K | $\Delta_f^g G_m^o(\theta)$/J·mol$^{-1}$ | $\Delta_f^g H_m^o(\theta)$/J·mol$^{-1}$ | $\Delta_f^g S_m^o(\theta)$/J·K$^{-1}$·mol$^{-1}$ | $r^2$ | $\Delta_f^g C_{p,m}^o$ ($T$ = 388 K)/J·K$^{-1}$·mol$^{-1}$ |
|---|---|---|---|---|---|---|
| | | | [$C_2C_1$im][Ntf$_2$] | | | |
| 445 to 483 | 464.36[a] | 58 683 ± 11 | 114 562 ± 445 | 120.4 ± 0.9 | 0.9997 | −112 |
| | 298.15 | 82 504 ± 1150 | 133 177 ± 930 | 170.0 ± 2.6 | | |
| | | | [$C_3C_1$im][Ntf$_2$] | | | |
| 453 to 493 | 473.04[a] | 56 926 ± 14 | 113 331 ± 539 | 119.3 ± 0.9 | 0.9996 | −117[b] |
| | 298.15 | 82 140 ± 884 | 133 793 ± 475 | 173.4 ± 2.8 | | |
| | | | [$C_4C_1$im][Ntf$_2$] | | | |
| 463 to 487 | 475.01[a] | 57 248 ± 7 | 117 752 ± 445 | 127.4 ± 0.8 | 0.9998 | −121 |
| | 298.15 | 84 374 ± 881 | 139 152 ± 470 | 183.8 ± 2.6 | | |
| | | | [$C_5C_1$im][Ntf$_2$] | | | |
| 457 to 493 | 474.99[a] | 57 479 ± 12 | 122 978 ± 526 | 138.0 ± 0.9 | 0.9997 | −127[b] |
| | 298.15 | 86 690 ± 893 | 145 437 ± 491 | 196.9 ± 2.8 | | |
| | | | [$C_6C_1$im][Ntf$_2$] | | | |
| 465 to 489 | 477.35[a] | 57 490 ± 16 | 126 053 ± 990 | 143.7 ± 1.9 | 0.9993 | −134 |
| | 298.15 | 88 438 ± 372 | 150 065 ± 798 | 206.9 ± 4.0 | | |
| | | | [$C_7C_1$im][Ntf$_2$] | | | |
| 465 to 493 | 478.92[a] | 58 085 ± 7 | 128 729 ± 387 | 147.6 ± 0.8 | 0.9999 | −138[b] |
| | 298.15 | 90 196 ± 887 | 153 675 ± 480 | 213.0 ± 2.4 | | |
| | | | [$C_8C_1$im][Ntf$_2$] | | | |
| 473 to 495 | 484.10[a] | 58 582 ± 12 | 128 608 ± 857 | 144.7 ± 1.8 | 0.9996 | −143 |
| | 298.15 | 91 406 ± 1222 | 155 199 ± 837 | 214.0 ± 3.7 | | |
| | | | [$C_{10}C_1$im][Ntf$_2$] | | | |
| 479 to 495 | 487.38[a] | 59 960 ± 5 | 136 028 ± 500 | 156.1 ± 0.9 | 0.9999 | −154[b] |
| | 298.15 | 96 071 ± 964 | 165 169 ± 573 | 231.8 ± 2.8 | | |
| | | | [$C_{12}C_1$im][Ntf$_2$] | | | |
| 481 to 493 | 486.85[a] | 61 731 ± 7 | 140 348 ± 809 | 161.5 ± 1.8 | 0.9998 | −165[b] |
| | 298.15 | 99 215 ± 1210 | 171 484 ± 815 | 242.5 ± 3.5 | | |

[a] Mean temperature. $r^2$ is the linear regression coefficient. [b] $\Delta_f^g C_{p,m}^o$(388 K) estimated using the linear fitted function ($\Delta_f^g C_{p,m}^o = -5.40\,n(C) - 100.47$) derived from fitting of the literature data of $\Delta_f^g C_{p,m}^o$(388 K) as a function of the cationic alkyl chain length. It was considered an uncertainty of 5 J·K$^{-1}$·mol$^{-1}$.

interactions arising from the increment of the −$CH_2$− group from [$C_2C_1$im][Ntf$_2$] to [$C_3C_1$im][Ntf$_2$] (further discussion follows).

The entropies of vaporization profile along the series in Figure 4 are analogous to those observed for the enthalpies of vaporization.

The results show a steady increase in $\Delta_f^g S_m^o$ along the homologous series and a trend shift in the increase in $\Delta_f^g S_m^o$ with $n$(C), around $n$(C) = 6, identical to that observed for the enthalpies of vaporization profile. Because the absolute standard molar entropies in the gaseous phase increase linearly along the homologous series,[22] the observed change should be due to an additional increase in the absolute entropy in the liquid phase, starting at [$C_6C_1$im][Ntf$_2$]. The derived results for the standard molar entropies of vaporization and the absolute standard molar entropies in the gaseous and liquid phases are presented in Table S3 of the Supporting Information.

The accuracy and resolution of these results for the extended series of [$C_nC_1$im][Ntf$_2$] are sufficient to demonstrate that the two (entropic and enthalpic) trend changes at $n$(C) = 6 compensate for each other and that there is a steady increase in the resulting Gibbs energy values from [$C_3C_1$im][Ntf$_2$] to [$C_{12}C_1$im][Ntf$_2$].

It is important to stress that previous studies, utilizing only a handful of cations with an even number of carbon atoms in the alkyl side chain, did not allow for a complete characterization of the important trend changes of the thermodynamic parameters of vaporization, including the outlier character of [$C_2C_1$im][Ntf$_2$], as evidenced in this work.

Figure 5 demonstrates the increments per −$CH_2$− group in the vaporization thermodynamic properties in the ILs and some alkyl derivatives.

It is interesting to observe that the ILs present a regular increase of (1.9 ± 0.1) kJ·mol$^{-1}$ per methylene group on the Gibbs energies of vaporization as compared with an increment of 2.86 kJ·mol$^{-1}$ observed on alkanes, 1-alcohols, and 1-amino alkanes.[26−28] The smaller increase in the Gibbs energies of vaporization of the ILs reflects the increase in the chemical potential of the liquid phase. This results from a balance between the decrease in the electrostatic potential and the increase in the nonelectrostatic interactions with the increase in the cationic alkyl chain length. The contribution per methylene unit to $\Delta_f^g H_m^o$(298.15

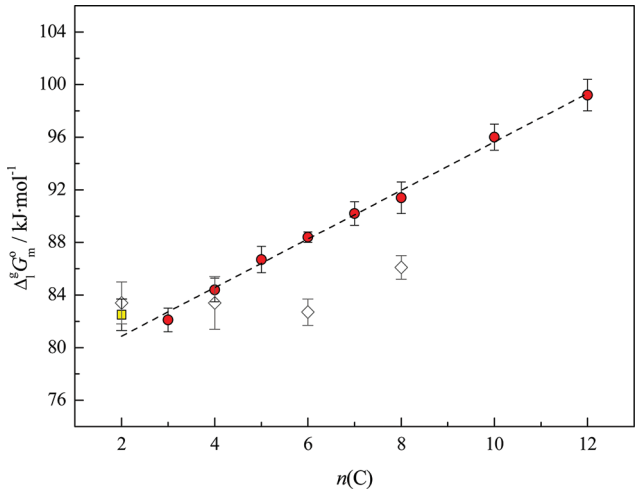


**Figure 2.** Graphic representation of standard molar Gibbs energies of vaporization at reference temperature ($T$ = 298.15 K) as a function of the number of carbon atoms in the alkyl side chain of the cation, $n$(C). □ (yellow),○ (red), this work (Knudsen effusion/quartz crystal microbalance method); ◇, Zaitsau et al.[12] (Knudsen effusion method).

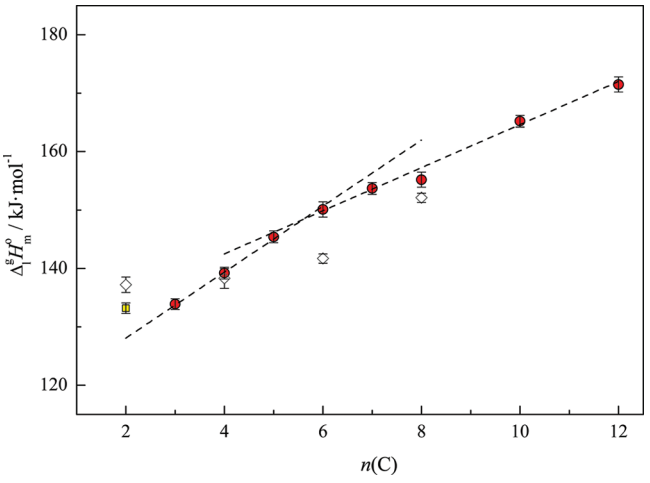


**Figure 3.** Graphic representation of standard molar enthalpies of vaporization at reference temperature ($T$ = 298.15 K) as a function of the number of carbon atoms in the alkyl side chain of the cation, $n$(C). □ (yellow), ○ (red), this work (Knudsen effusion/quartz crystal microbalance method); ◇, Zaitsau et al.[12] (Knudsen effusion method).

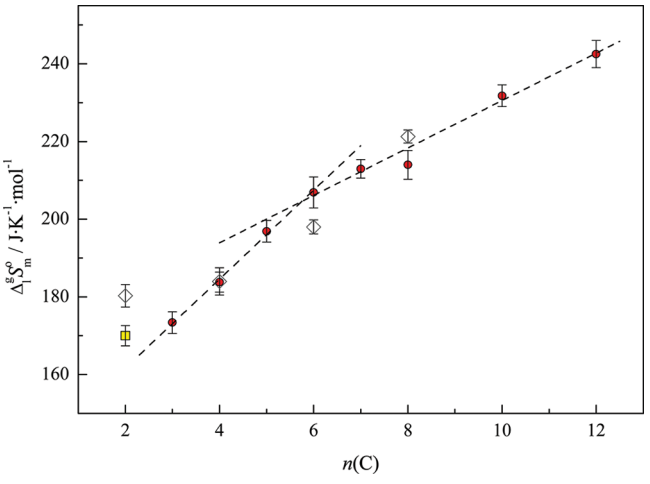


**Figure 4.** Graphic representation of standard molar entropies of vaporization, at reference temperature ($T$ = 298.15 K), as a function of the number of carbon atoms in the alkyl side chain of the cation, $n$(C). □, (yellow), ○ (red), this work (Knudsen effusion/Quartz crystal microbalance method); ◇, Zaitsau et al.[12] (Knudsen effusion method).

K), in the range from $[C_3C_1im][Ntf_2]$ to $[C_6C_1im][Ntf_2]$, is comparable to that observed for the liquid phase in the alkyl derivatives and decreases after $[C_6C_1im][Ntf_2]$, directly reflecting the regular decrease in the electrostatic interaction; it indicates the beginning of a new regular type of molecular interaction.

The relatively smaller increase per methylene unit to the entropy of vaporization of the ILs as compared with the increment observed for the alkyl derivatives from $[C_3C_1im][Ntf_2]$ to $[C_6C_1im][Ntf_2]$ must be related to the decrease in rotational entropy contribution of the alkyl groups in the region of strong electrostatic interaction. The profile of the $\Delta_l^g S_m^o$ trend in the series, above $[C_6C_1im][Ntf_2]$, is identical to that observed in the alkyl derivatives and is identical to those observed along the alkane homologous series.

The enthalpic and entropic vaporization trend changes along the $[C_nC_1im][Ntf_2]$ series and must be related to a change in the molecular structure of the liquid phase around $[C_6C_1im][Ntf_2]$. The existing models for the structure of ionic liquids at a molecular level consider them to be nanosegregated fluids. To evaluate if this nanosegregation might be related to the trend changes observed in the thermodynamic properties of vaporization, we carried out MD studies for the $[C_nC_1im][Ntf_2]$ ionic liquid series. These MD studies[29−31] and subsequently X-ray diffraction studies[32] recognized the nanosegregated structures of ionic liquids. Although those first studies focused on the 1-alkyl-3-methylimidazolium hexafluorophosphate series, $[C_nC_1im][PF_6]$, the conclusions were quickly extended to the $[C_nC_1im][Ntf_2]$ series and contained two basic types of conclusion: (i) ionic liquids are highly structured fluids composed of high-charge density areas (the "polar heads" of the anions and cations forming a polar network) permeated by low-charge density regions (the alkyl side chains present in some of the ions forming nonpolar domains); (ii) the topology of the nonpolar domains is strongly dependent on the relative volumes occupied by the polar and nonpolar moieties of the molecules. For very small alkyl side chains, the nonpolar domains are isolated islands in a continuous polar domain; for longer alkyl side chains, those islands start to coalesce, and after a certain threshold value is reached, they form a second, continuous nonpolar domain. This corresponds to a kind of percolation limit of the nonpolar network regions and the formation of a bicontinuous fluid phase.[31,33]

The trend shifts observed for $\Delta_l^g H_m^o$ and $\Delta_l^g S_m^o$ as a function of the cationic alkyl side chain length (Figures 3 and 4) are related to the structural modifications that occur when the number of alkyl carbon atoms nears six.

For the $[C_nC_1im][PF_6]$ ionic liquids,[31,32] the percolation limit of the nonpolar islands was found to occur around $n$(C)= 4 to 5. With bulkier anions like $[Ntf_2]^-$ and a concomitantly larger polar network, as can be inferred from Figure S5 (Supporting Information), this threshold value was predicted to be larger.[33] New simulation runs were performed for all $[C_nC_1im][Ntf_2]$ ionic liquids between $n$(C)= 2 and 10, in order to verify if the

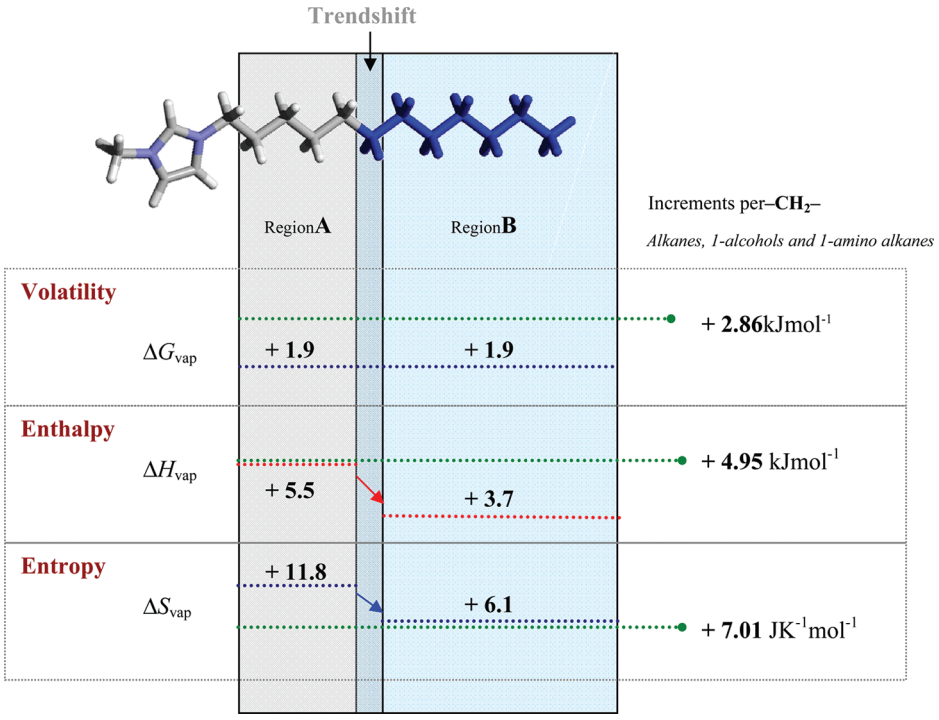


**Figure 5.** Schematic comparative diagram of the increments per methylene group of the thermodynamic vaporization properties between the studied ILs (before and after the trend shift $n$(C)) and the typical alkane derivatives data.[26−28]

percolation limit was attained around $n$(C)= 6, as occurred for the $\Delta_l^g H_m^o[n(C)]$ and $\Delta_l^g S_m^o[n(C)]$. Figure 6 shows the CT−CT radial distribution functions for the different ionic liquids and two snapshots of the simulation boxes for $[C_4C_1im][Ntf_2]$ and $[C_8C_1im][Ntf_2]$ (CT, carbons of the terminal methyl groups of the chain).

All RDFs show an intense first peak that tends to be higher as the alkyl side chain gets longer; that is, the terminal carbon atoms of the alkyl side chains tend to separate from the polar regions of the ionic liquid and come to rest in proximity to each other. This is particularly true for ionic liquids from $[C_2C_1im][Ntf_2]$ to $[C_5C_1im][Ntf_2]$, where the small clusters (islands) containing the adjoining CT groups (cf. circled areas in Figure 6a) are growing. However, above a certain alkyl side chain length (around $[C_6C_1im][Ntf_2]$), the intensities of the first peaks start to become almost constant. This suggests that to segregate from the nonpolar network, the CT atoms do not have to form a small cluster (the percolation limit was reached and a more ample and continuous nonpolar region is now available) and that the first peak intensities tend to increase because of the overall decrease in the volume fraction of the CT groups. (Radial distribution functions are normalized taking into account the average density of the pair under scrutiny in the total system volume.) Additionally, the structural modification from small clusters to a continuous nonpolar nanophase can be ascertained from a new type of analysis based on the second peaks: a string of CT atoms like those depicted in Figure 6b will exhibit shorter second neighbor distances than those found between CT atoms from neighboring, independent clusters. This is indeed the situation observed in the RDFs from $[C_4C_1im][Ntf_2]$ to $[C_{10}C_1im][Ntf_2]$: the peak around 1 nm in $[C_4C_1im][Ntf_2]$ starts decreasing and shifting in $[C_5C_1im][Ntf_2]$ and forms an incipient peak at 0.8 nm (twice the distance of the first peak at 0.4 nm) in $[C_6C_1im][Ntf_2]$, which then grows continuously from $[C_7C_1im][Ntf_2]$ to $[C_{10}C_1im][Ntf_2]$.

The simulations show a structural shift around $[C_6C_1im]$-$[Ntf_2]$ when the nonpolar island percolation limit is reached for this series of ionic liquids. This is consistent with higher $S_m^o(l)$ values from $[C_6C_1im][Ntf_2]$ onward, as inferred from the experimental results of this work (Figure 4). For $n$(C) > 6, the absolute entropy in the liquid phase increases more rapidly as the distances and segregation between the terminal alkyl groups and polar domains increase and the corresponding interactions decrease. The same argument also justifies the trend found for the cohesive energy of the liquid phase (Figure 3).

The $[C_2C_1im][Ntf_2]$ outlier character can also be analyzed taking into account possible structural changes occurring in the liquid phase, as evidenced by other simulation studies. (See the Supporting Information.)

The relation between the $\Delta_l^g H_m^o$ and $\Delta_l^g S_m^o$ trends and the structural changes in the liquid phase observed for the $[C_nC_1im][Ntf_2]$ series shed further light on recently reported experimental viscosity data and their temperature dependence for this same series of ionic liquids.[34] Figure 7 shows the trends of the viscosity and the corresponding parameters ($A$, $E$) of the Vogel−Tammann−Fulcher (VTF) equation used to fit the temperature dependence of the viscosity data along the $[C_nC_1im][Ntf_2]$ series. (See the details in the Supporting Information.) The Figure also clearly shows changes around $[C_6C_1im][Ntf_2]$.

The particularly conspicuous change observed in the pre-exponential factor of the VTF equation, $A$, around $[C_6C_1im]$ $[Ntf_2]$ indicates (and is in agreement with) an additional increase in liquid phase entropy. On the other hand, the decrease in the change of cohesive energies is only slightly reflected in the decrease of the viscosity activation energy, $E$. Interestingly, $[C_2C_1im][Ntf_2]$

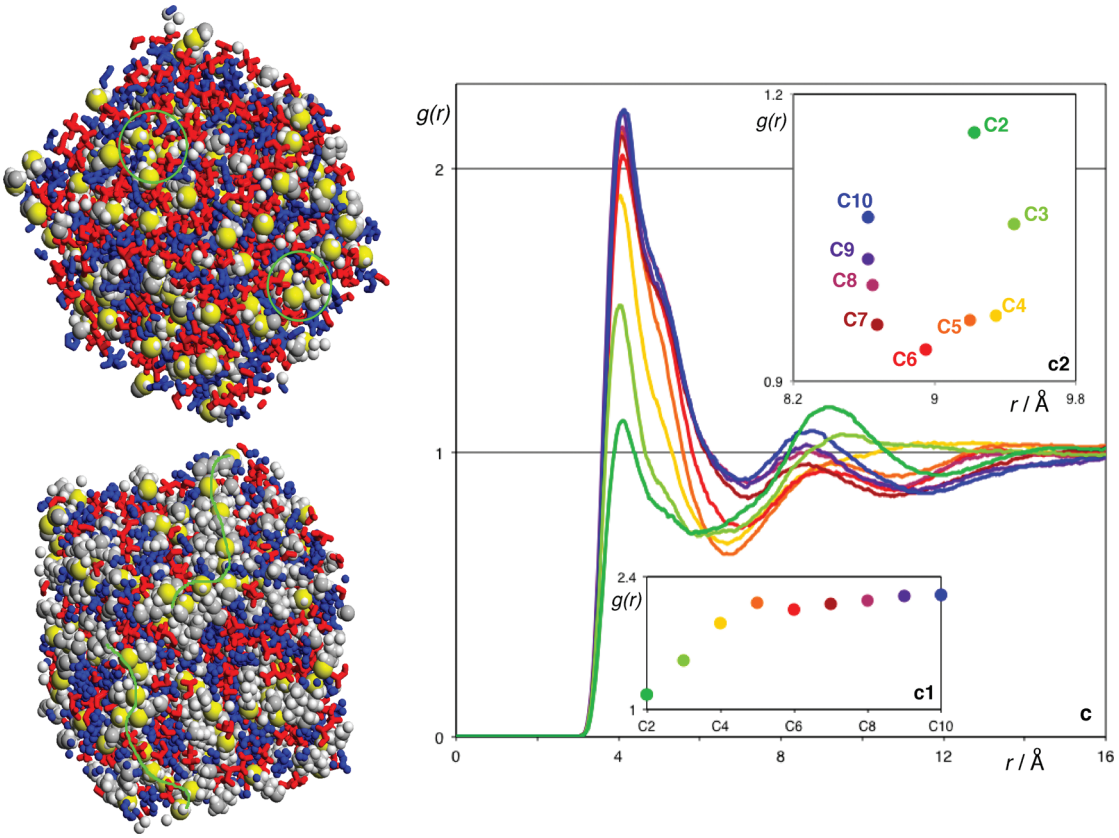


**Figure 6.** Two snapshots of simulation boxes containing $[C_4C_1im][Ntf_2]$ (top) and $[C_8C_1im][Ntf_2]$ ionic liquids (bottom). The high-charge density regions of the cations and anions are colored as blue and red sticks to highlight the continuity of the polar network. The alkyl side chains (from C2 onward) are colored using space-filled atoms and the SPK convention (carbon, gray; hydrogen, white). The terminal atoms (CT) of each alkyl side chain are colored in yellow and given a larger space filling radius. The green lines emphasize the relations between the CT atoms, as discussed in the text. The CT−CT radial distribution functions of all $[C_nC_1im][Ntf_2]$ ($n$ = 2−10) are given next to the snapshots.

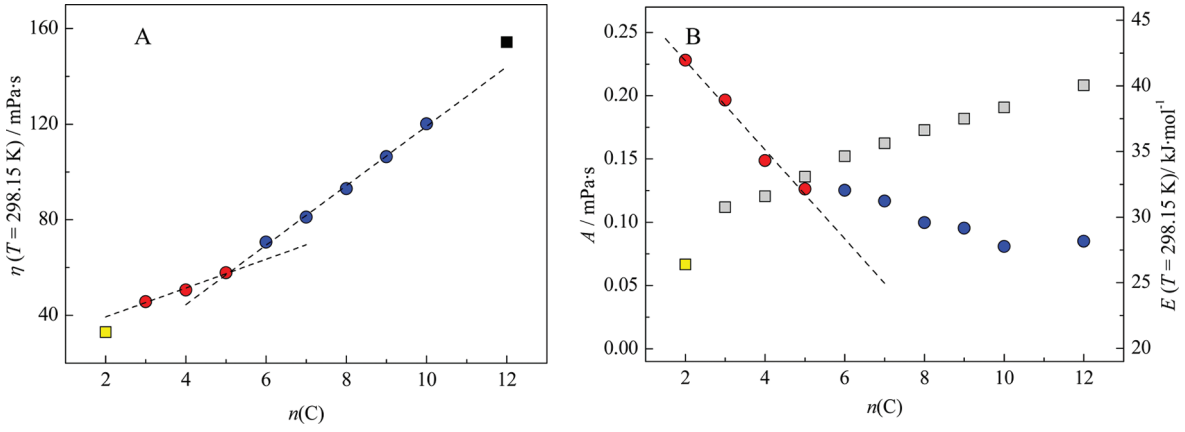


**Figure 7.** Plots of viscosity ($\eta$/mPa·s) at $T$ = 298.15 K, pre-exponential coefficient of the Vogel−Tammann−Fulcher equation ($A$/mPa·s), and activation energy ($E$/kJ·mol$^{-1}$) at $T$ = 298.15 K as a function of the number of carbon atoms in the alkyl side chain of the cation, $n$(C). (B) □ (yellow), □ (gray), $E$/kJ·mol$^{-1}$; ○ (red), ○ (blue), $A$/mPa·s. Derived from the data presented in ref 34.

is again an outlier relative to the rest of the homologous series. In this case, however, its varying viscosity is dominated by a significant lower contribution from its activation energy.

## 4. FINAL REMARKS

The study of the nine imidazolium-based ionic liquids enabled us to detect important trends in the thermodynamic parameters, which would have been impossible to verify with a smaller number of ILs. The high accuracy and resolution of the present vapor pressure results were sufficient to extract the individual thermodynamic entropic and enthalpic contributions to the liquid−vapor equilibrium.

The thermodynamic results herein reported constitute the first experimental quantitative evidence of the structural percolation


dx.doi.org/10.1021/jp2049316 |J. Phys. Chem. B 2011, 115, 10919–10926

phenomenon and represent an important contribution to increased understanding of the relationship between ionic liquids, cohesive energies, volatility and liquid structures. They also clarify the existent discrepancy between the thermodynamic properties of vaporization encountered in the literature and consequently provide strong experimental validation of the accurate parametrization of molecular force fields used in computer simulations.

## ■ ASSOCIATED CONTENT

**Supporting Information.** Experimental vapor pressures for the nine imidazolium-based ILs; literature data regarding heat capacities in the gaseous and liquid phases together with the calculated values, comparisons of the vapor pressures and enthalpies of vaporization with literature data, absolute standard molar entropies in gaseous and liquid phases, and molecular dynamics results. This material is available free of charge via the Internet at http://pubs.acs.org.

## ■ AUTHOR INFORMATION

**Corresponding Author**
*Tel: +351 220 402 836. Fax: +351 220 402 659. E-mail: lbsantos@fc.up.pt.

## ■ ACKNOWLEDGMENT

This work was supported by the *Fundação para a Ciência e a Tecnologia*. B.S., K.S., C.F.R.A.C.L., and M.A.A.R. acknowledge the financial support from *Fundação para a Ciência e a Tecnologia* for the research grants, specifically: SFRH/BPD/38637/2007, SFRH/BPD/38339/2007, SRFH/BD/29394/2006, and SFRH/BD/60513/2009, respectively. We also thank FCT for financial support for the project PTDC/QUI/72903/2006.

## ■ REFERENCES

(1) Greaves, T. L.; Drummond, C. J. *Chem. Rev.* **2008**, *108*, 206–237.
(2) Plechkova, N. V.; Seddon, K. R. *Chem. Soc. Rev.* **2008**, *37*, 123–150.
(3) Swatloski, R. P.; Spear, S. K.; Holbrey, J. D.; Rogers, R. D. *J. Am. Chem. Soc.* **2002**, *124*, 4974–4975.
(4) Ohno, H.; Fukaya, Y. *Chem. Lett.* **2009**, *38*, 2–7.
(5) Wu, B.; Reddy, R. G.; Rogers, R. D. Novel Ionic Liquid Thermal Storage for Solar Thermal Electric Power Systems, Proceedings of the Solar Forum 2001, Washington, D.C., 2001.
(6) Zhao, D.; Liao, Y.; Zhang, Z. *Clean* **2007**, *35*, 42–48.
(7) Scammells, P. J.; Scott, J. L.; Singer, R. D. *Aust. J. Chem.* **2005**, *58*, 155–169.
(8) Earle, M. J.; Esperança, J. M. S. S.; Gilea, M. A.; Canongia Lopes, J. N.; Rebelo, L. P. N.; Magee, J. W.; Seddon, K. R.; Widegren, J. A. *Nature* **2006**, *439*, 831–834.
(9) MacFarlane, D. R.; Pringle, J. M.; Johansson, K. M.; Forsyth, S. A.; Forsyth, M. *Chem. Commun.* **2006**, 1905–1917.
(10) Esperança, J. M. S. S.; Canongia Lopes, J. N.; Tariq, M.; Santos, L. M. N. B. F.; Magee, J. W.; Rebelo, L. P. R. *J. Chem. Eng. Data* **2010**, *55*, 3–12.
(11) Köddermann, T.; Paschek, D.; Ludwig, R. *Chem. Phys. Chem.* **2007**, *8*, 2464–2470.
(12) Zaitsau, D. H.; Kabo, G. J.; Strechan, A. A.; Paulechka, Y. U.; Tschersich, A.; Verevkin, S. P.; Heintz, A. *J. Phys. Chem. A* **2006**, *110*, 7303–7306.
(13) Emel'yanenko, V. N.; Verevkin, S. P.; Heintz, A. *J. Am. Chem. Soc.* **2007**, *129*, 3930–3937.
(14) Armstrong, J. P.; Hurst, C.; Jones, R. G.; Licence, P.; Lovelock, K. R. J.; Satterley, C. J.; Villar-Garcia, I. J. *Phys. Chem. Chem. Phys.* **2007**, *9*, 982–990.
(15) Deyko, A.; Lovelock, K. R. J.; Corfield, J.-A.; Taylor, A. W.; Gooden, P. N.; Villar-Garcia, I. J.; Licence, P.; Jones, R. G.; Krasovskiy, V. G.; Chernikova, E. A.; Kustov, L. M. *Phys. Chem. Chem. Phys.* **2009**, *11*, 8544–8555.
(16) Santos, L. M. N. B. F.; Canongia Lopes, J. N.; Coutinho, J. A. P.; Esperanca, J. M. S. S.; Gomes, L. R.; Marrucho, I. M.; Rebelo, L. P. N. *J. Am. Chem. Soc.* **2007**, *129*, 284–285.
(17) Luo, H.; Baker, G. A.; Dai, S. *J. Phys. Chem. B* **2008**, *112*, 10077–10081.
(18) Santos, L.M.N.B.F.; Lima, L. M. S. S.; Lima, C.F.R.A.C.; Magalhães, F. D.; Torres, M. C.; Schröder, B.; Ribeiro da Silva, M. A. V. *J. Chem. Thermodyn.* **2011**, *43*, 834–843.
(19) Bonhôte, P.; Dias, A. P.; Armand, M.; Papageorgiou, N.; Kalyanasundaram, K.; Grätzel, M. *Inorg. Chem.* **1996**, *35*, 1168–1178.
(20) Wieser, M. E.; Berglund, M. *Pure Appl. Chem.* **2009**, *81*, 2131–2156.
(21) Clarke, E. C. W.; Glew, D. N. *Trans. Faraday Soc.* **1966**, *62*, 539–547.
(22) Paulechka, Y. U.; Kabo, G. J.; Emel'yanenko, V. N. *J. Phys. Chem. B* **2008**, *112*, 15708–15717.
(23) Blokhin, A. V.; Paulechka, Y. U.; Kabo, G. J. *J. Chem. Eng. Data* **2006**, *51*, 1377–1388.
(24) Paulechka, Y. U.; Blokhin, A. V.; Kabo, G. J.; Strechan, A. A. *J. Chem. Thermodyn.* **2007**, *39*, 866–877.
(25) Blokhin, A. V.; Paulechka, Y. U.; Strechan, A. A.; Kabo, G. J. *J. Phys. Chem. B* **2008**, *112*, 4357–4364.
(26) Růžička, K.; Majer, V. *J. Phys. Chem. Ref. Data* **1994**, *23*, 1–39.
(27) Matulis, D. *Biophys. Chem.* **2001**, *93*, 67–82.
(28) Chickos, J. S.; Hanshaw, W. *J. Chem. Eng. Data* **2004**, *49*, 77–85.
(29) Urahata, S. M.; Ribeiro, M. C. C. *J. Chem. Phys.* **2004**, *120*, 1855–1863.
(30) Wang, Y.; Voth, G. A. *J. Am. Chem. Soc.* **2005**, *127*, 12192–12193.
(31) Canongia Lopes, J. N.; Pádua, A. A. H. *J. Phys. Chem. B* **2006**, *110*, 3330–3335.
(32) Triolo, A.; Russina, O.; Bleif, H.-J.; Di Cola, E. *J. Phys. Chem. B* **2007**, *111*, 4641–4644.
(33) Shimizu, K.; Gomes, M. F. C.; Pádua, A. A. H.; Rebelo, L. P. N.; Canongia Lopes, J. N. *THEOCHEM* **2010**, *946*, 70–76.
(34) Tariq, M.; Carvalho, P. J.; Coutinho, J. A.P.; Marrucho, I. M.; Canongia Lopes, J. N.; Rebelo, L. P.N. *Fluid Phase Equilib.* **2011**, *301*, 22–32.